Ocean Systems Engineering, *Vol. 15, No. 4 (2025) 423-439*
https://doi.org/10.12989/ose.2025.15.4.423

Computational analysis of underlip geometry and power take-off damping effects on oscillating water column performance

Muhammad A. Bramantya*[1], Heru S.B. Rocharjo[1a], Ayodya P. Tenggara[2b] and Rahmawan Budiarto[2c]

[1]*Department of Mechanical and Industrial Engineering, Faculty of Engineering, Gadjah Mada University, Jl. Grafika 2, Yogyakarta 55281, Indonesia*
[2]*Department of Nuclear Engineering and Engineering Physics, Faculty of Engineering, Gadjah Mada University, Jl. Grafika 2, Yogyakarta 55281, Indonesia*

(Received August 14, 2025, Revised December 2, 2025, Accepted December 7, 2025)

Abstract. The geometry of the underlip in onshore oscillating water column (OWC) systems is a key determinant of their hydrodynamic performance, directly influencing the wave-structure interactions and energy conversion efficiency. Recent advances in experimental hydrodynamics have highlighted the potential of geometric optimization; however, the specific influence of underlip configurations remains underexplored in the context of high-fidelity computational modeling. This study addresses this gap by performing a systematic evaluation of multiple underlip geometries using computational fluid dynamics (CFD) simulations. The analysis revealed that subtle geometric modifications could yield substantial performance gains. Notably, the circular underlip configuration achieved the highest improvement, enhancing the efficiency by 9.1% under a takeoff damping variation of 0.0079. This improvement was attributed to its capacity to suppress turbulent kinetic energy generation during wave impact, thereby reducing energy dissipation. The results present a novel, cost-effective design optimization pathway that requires minimal structural modification, contributing to the growing body of research on hydrodynamic enhancement strategies for OWC-based wave energy converters.

Keywords: computational fluid dynamic; hydrodynamic; oscillating water column; underlip geometry; wave conversion energy

1. Introduction

The geometry of oscillating water column (OWC) wave energy converters has a profound influence on hydrodynamic performance because it governs internal flow characteristics and thus determines the efficiency of wave energy capture. The geometric configuration affects the interaction between the incident waves and chamber, shaping the fluid transport patterns and energy transfer to the power take-off (PTO) system. Consequently, optimizing the OWC geometry

*Corresponding author, Ph.D., E-mail: bramantya@ugm.ac.id
[a] Professor, E-mail: heru-sbr@ugm.ac.id
[b] Ph.D., E-mail: ayodya.p.t@ugm.ac.id
[c] Ph.D., E-mail: rachmawan@ugm.ac.id

http://www.techno-press.org/?journal=ose&subpage=7 ISSN: 2093-6702 (Print), 2093-677X (Online)

is a critical strategy for enhancing the energy conversion efficiency, often with designs tailored to match site-specific wave climates.

Extensive research has demonstrated that even modest geometric variations can significantly influence the OWC performance. Mohapatra *et al*. (2023) highlighted that the underlying chamber geometry plays a pivotal role in controlling the fluid transport near the front wall, which is the primary zone for energy capture. Building on this foundation, several studies have examined structural modifications of the OWC front wall to optimize the hydrodynamic response. Qu *et al.* (2022) investigated offshore OWC devices with elliptical front walls at varying inclination angles, reporting maximum efficiency at an elliptic angle of 25°, attributed to improved wave focusing and reduced energy loss. Similarly, Fleming and Macfarlane (2017) explored the upper and lower lip opening angles and concluded that sharp geometries induce vorticity and turbulence detrimental to efficiency, while widening the upper lip angle can enhance energy capture. Carlo *et al*. (2023) proposed a U-shaped front wall to dissipate excessive wave energy before chamber entry, thereby improving internal resonance conditions.

While these large-scale interventions have shown measurable benefits, other studies have revealed that relatively simple geometric changes can yield disproportionately high efficiency gains. Mandev and Altunkaynak (2023) experimentally demonstrated that attaching cylindrical structures to the underlip of an OWC improved the efficiency by 45% compared to a conventional rectangular baseline. Likewise, Çelik (2022) assessed several underlip geometries and identified the cylindrical configuration as the most effective, with a maximum improvement of 21.1%. These findings underscore that underlip geometry, although often overlooked, plays a critical role in shaping the flow dynamics, turbulence characteristics, and energy dissipation patterns within the chamber.

Recent research has emphasized the necessity of treating the internal hydrodynamics of oscillating water column (OWC) devices and the characteristics of the power take-off (PTO) system as a coupled design problem rather than isolated subsystems. Empirical investigations of a maritime natural cave acting as a full-scale OWC analog have shown that the flow contraction induced by an orifice or Wells turbine defines an optimal damping range that maximizes pneumatic power, whereas suboptimal PTO configurations can substantially reduce overall energy capture even under favorable wave conditions by Monteiro et al. (2025). From a design standpoint, high-fidelity computational fluid dynamics (CFD) simulations of single- and multi-chamber OWCs, combined with machine learning surrogate models, have been used to explore wide design spaces in chamber geometry, orifice sizing, and wave parameters, thereby identifying configurations that enhance hydrodynamic efficiency and broaden the effective operating bandwidth by Prasanna *et al.* (2025). Complementary time-domain simulations in irregular seas have further clarified how pneumatic and viscous losses in the air duct can be represented by equivalent linear damping models and how these losses interact with internal free-surface resonance to shape the device response by Koo and Kim (2012). Collectively, these studies indicate that the performance of an OWC is highly sensitive to the interaction between the geometric features in the entrance region, internal resonance characteristics, and PTO damping.

Building on this system-level perspective, recent studies have demonstrated that the geometry of the OWC chamber, particularly near the wave entrance, exerts a decisive influence on energy capture when considered jointly with PTO characteristics. Numerical investigations of offshore OWCs have shown by Mia *et al.* (2022) that adjustments to the front and rear wall draughts and the inclusion of a bottom plate can significantly modify the hydrodynamic efficiency and internal resonance, underscoring the importance of the entrance and submergence configuration.

Experimental studies on sloping-wall devices by Mandev and Altunkaynak (2023) indicate that streamlining the chamber front face reduces vortex shedding and viscous losses, shifts the optimal PTO damping towards higher damping levels, and broadens the effective operating range. More specifically, cylindrical front-wall entrance (underlip) geometries have been reported to enhance the capture width ratio by up to approximately 45% relative to sharp-edged baselines, with the optimal cylinder diameter depending on the dimensionless wavenumber and PTO orifice ratio, highlighting a strong interaction between the underlip shape and damping conditions. Complementary CFD studies of novel onshore front-wall configurations by Güths *et al*. (2022) have shown that carefully tailored external and internal wall slopes can reduce wave reflection and run-up while maintaining or improving pneumatic energy extraction, emphasizing the central role of entrance shaping in the global energy balance.

Beyond entrance shaping and chamber streamlining, several recent studies have more broadly highlighted that the internal dynamics of an OWC are governed by a delicate interplay between the underwater opening geometry, bottom profile, and PTO damping. Detailed flume experiments have shown that variations in the relative front-wall opening and orifice ratio strongly affect water-column displacement, air pressure build-up, and sloshing behavior, leading to the introduction of compact dimensionless groups that couple wave frequency, opening ratio, and pneumatic damping into a single predictive metric by Çelik and Altunkaynak (2021). Analytical work on devices with surging front and rear lip-walls by Wang *et al*. (2022) has demonstrated that mechanically tuned movable entrances can exceed the classical linear efficiency limit and broaden the effective operating bandwidth when their stiffness is co-optimized with the PTO characteristics. Simultaneously, nonlinear time-domain simulations of multi-OWC platforms using higher-order boundary element methods have clarified how nonlinear PTO damping and internal free-surface dynamics interact in three dimensions, with array layout and directional spreading exerting a strong influence on the capture width by Zhou *et al*. (2021). Complementary experimental investigations of different internal bottom profiles by Ashlin *et al.* (2016) indicate that curved chamber floors can enhance wave amplification and hydrodynamic efficiency relative to flat or simply sloping bases by moderating flow separation and dissipation within the cavity. Taken together, these contributions underscore that the OWC entrance region and internal geometry must be tuned jointly with PTO damping; however, the specific role of fixed underlip geometry, which is distinct from general opening height, movable lip walls, or bottom profiling, and its coupled interaction with PTO damping remain insufficiently explored in a computational framework, providing the motivation for the present study.

Despite these advances, there remains a limited understanding of the detailed hydrodynamic mechanisms through which the underlip geometry affects OWC performance, particularly under varying PTO damping conditions. Most prior studies have relied on experimental approaches, which, while valuable, offer a limited resolution of the internal flow fields. Computational fluid dynamics (CFD) is a powerful complementary tool that enables the detailed analysis of wave–structure interaction, turbulent kinetic energy distribution, and chamber resonance effects under controlled geometric variations.

In light of these gaps, the present study employed CFD simulations to systematically investigate the influence of underlip geometry on the performance of an onshore OWC device. Five alternative configurations (rounded, quarter-circle, semicircle back, circular, and semicircle front) were compared against a conventional rectangular underlip model. The simulations were conducted under varying PTO damping coefficients and validated against the experimental results from Çelik (2022) to ensure model fidelity. The objectives are twofold: (i) to quantify the

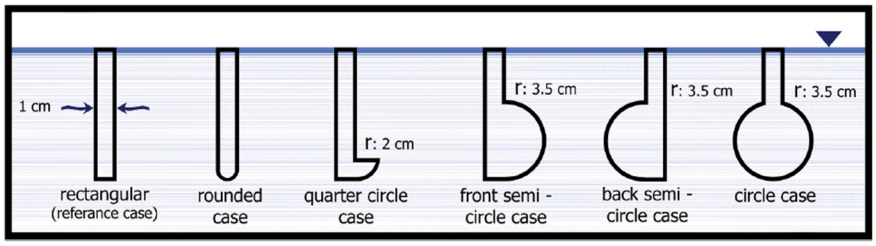

Fig. 1 Modification of underlip model

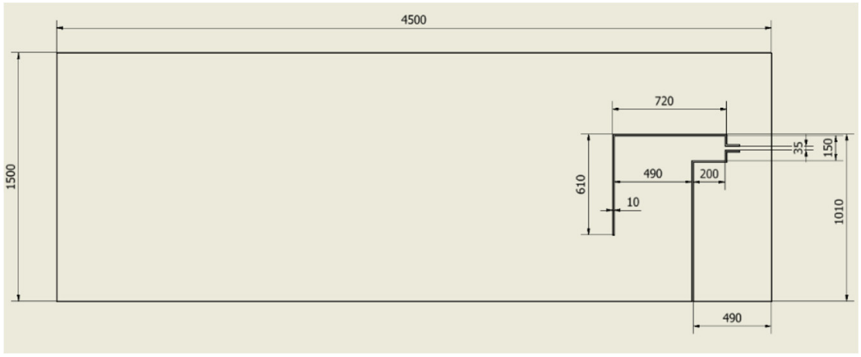

Fig. 2 Model of geometry domain

efficiency gains achievable through small-scale underlip modifications and (ii) to elucidate the hydrodynamic mechanisms, particularly turbulence suppression and flow alignment, which underpin these improvements. By focusing on a design element that can be modified with minimal structural intervention, this study aims to provide a practical and cost-effective pathway for enhancing the OWC performance in real-world applications. The geometric configurations investigated in this study are shown in Fig. 1.

2. Simulation of oscillating water column

The numerical simulations in this study were conducted using ANSYS Fluent 2020 R2 software. Model verification and validation were performed against experimental data reported by Çelik (2022). The simulations were carried out in transient mode over a total duration of 200 s, with a time-step size of 0.05 s and a maximum of 20 iterations permitted per time step.

2.1 Computational domain and meshing

The computational domain was developed using ANSYS SpaceClaim. A two-dimensional (2D) configuration was adopted to improve the computational efficiency while maintaining solution fidelity. Previous work by Kamath *et al.* (2014) demonstrated that the hydrodynamic behavior in oscillating water column (OWC) systems is comparable between two-dimensional and

Fig. 3 Layout of mesh zone

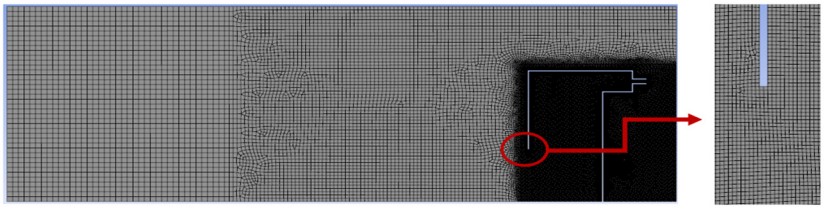

Fig. 4 Example of mesh

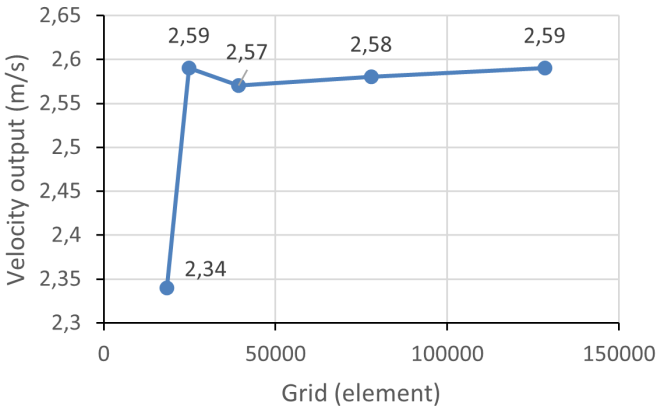

Fig. 5 Mesh independency test

three-dimensional (3D) models, thereby justifying the use of a 2D approach in the present study. The geometric dimensions of the domain were adapted from the experimental setup of Çelik (2022) to ensure consistency and to facilitate validation (Fig. 2).

Meshing was performed by using configurations tailored to each geometric variation. The mesh layout of the rectangular underlip model is illustrated in Fig. 3. The domain was divided into three distinct zones (Zone A, Zone B, and Zone C) to enable the application of the multizone meshing method. This segmentation allowed each zone to be assigned an appropriate mesh type and

resolution, according to its role in the simulation. The generated mesh is shown in Fig. 4.

Zone A was assigned a structured mesh to accommodate dynamic meshing operations because this region underwent mesh deformation during the simulation process. Zone B was meshed using a face size of 25 mm, balancing the computational cost and accuracy in a region of relatively low flow complexity. The mesh density for Zone C was determined through a mesh independence study, in which element sizes of 3, 4, 6, 8, and 10 mm were evaluated. As illustrated in Fig. 5, the variation in the simulation results beyond a mesh size of 3 mm was negligible, and this resolution was selected to ensure numerical accuracy without excessive computational demands.

This meshing strategy, although less complex than fully blocked grids, yielded results consistent with those of more intricate approaches, providing a robust and efficient foundation for subsequent CFD simulations.

2.2 Governing equation

The equations employed in this simulation were adapted from existing experimental cases to ensure consistency and comparability of the results. The formulation is based on the built-in models available in ANSYS Fluent, with the addition of wave-generation equations to represent the incident waves within the fluid domain. The primary governing equations include continuity, momentum conservation, and multiphase flow equations. According to ANSYS Inc. (2022), the continuity and momentum equations are expressed in Eqs. (1) and (2), respectively. The mixture density and viscosity are defined by Eqs. (3) and (4), respectively.

The mixture model was selected over the volume of fluid (VOF) model because it allows the simultaneous tracking of both phase velocities, which is particularly suitable for oscillating water column (OWC) simulations where detailed velocity field interactions are required. The theoretical justification for this approach lies in the ability of the model to resolve distinct phase velocities within a shared computational framework, enabling an accurate representation of air–water interactions in the OWC chamber.

In this study, both water and air within the chamber were modeled using an incompressible flow formulation. This modeling approach is consistent with the methodology employed by Vyzikas *et al.* (2017). The primary distinction lies in our implementation of the governing equations within the standard mixture model framework available in ANSYS Fluent, whereas the sliding-mesh wave maker is executed through a user-defined motion.

The turbulence was modeled using the Shear Stress Transport (SST) k–ω model. This choice was motivated by its proven accuracy in resolving near-wall flow features, particularly in regions of high shear, such as the underlip wall. Zeng *et al.* (2022) compared the k–ε and k–ω models in OWC numerical studies and concluded that the SST k–ω formulation provides the highest accuracy and is therefore recommended for such applications.

For the pressure–velocity coupling, the SIMPLE algorithm with second-order upwind discretization was employed. Although the PIMPLE scheme—a hybrid of the PISO and SIMPLE algorithms—has been used in other OWC studies e.g., Ning *et al*. (2023), it incurs a significantly higher computational cost. In the present case, the SIMPLE scheme demonstrated stable convergence across all iterations, making it a more efficient choice without compromising the accuracy.

$$\frac{\partial}{\partial x}(\rho_m) + \nabla.(\rho_m \vec{v}_m) = 0 \tag{1}$$

$$\frac{\partial}{\partial t}(\rho_m \vec{v}_m) + \nabla.(\rho_m \vec{v}_m \vec{v}_m) = -\nabla \mathrm{p} + \nabla.[\mu_m(\nabla \vec{v}_m + \nabla \vec{v}_m^T)] + \rho_m \vec{g} + \vec{F} - \nabla.\left(\sum_{k=1}^{n} \alpha_k \rho_k \vec{v}_{dr,k}\right) \quad (2)$$

$$\rho_m = \sum_{k=1}^{n} \alpha_k \rho_k \quad (3)$$

$$\mu_m = \sum_{k=1}^{n} \alpha_k \mu_k \quad (4)$$

$$\vec{v}_m = \frac{\sum_{k=1}^{n} \alpha_k \rho_k \vec{v}_k}{\rho_m} \quad (5)$$

$$\vec{v}_{dr,k} = \vec{v}_k - \vec{v}_m \quad (6)$$

where

ρ_m = mixture density (kg/m^3)
ρ_k = density of phase k (kg/m^3)
$\vec{v}_m$ = mixture velocity (m/s)
$\vec{v}_k$ = velocity of phase k (m/s)
$\vec{v}_{dr,k}$ = drift (slip) velocity of phase k relative to the mixture (m/s)
μ_m = mixture dynamic viscosity (Pa.s)
μ_k = dynamic viscosity of phase k (Pa.s)
g = gravitational (m/s^2)
$\vec{F}$ = external body-force (N/m^3)
α_k = volume fraction of phase k (ratio of phase volume to cell volume)

2.3 Boundary conditions

The specifications of the boundary conditions in oscillating water column (OWC) simulations must be consistent with the experimental setup and the physical model being reproduced. An accurate definition of these boundaries is critical because it determines the validity of the hydrodynamic interactions within the computational domain. The boundary configuration adopted in this study is illustrated in Fig. 6 and Table 1.

Because the simulation was conducted in two dimensions, the computational domain comprised five boundary segments. The top boundary (labelled top) is defined as a pressure outlet condition that allows free passage of air and pressure fluctuations. The bottom, far-field, and column wall boundaries were assigned no-slip conditions to replicate the physical constraints of the structure. The wave-generating boundary was implemented as a sliding wall condition, driven by a regular wave function to replicate incident ocean waves. This approach follows the sliding plane method used in experimental wave flume studies.

Prior to initialization, the domain is divided into two regions and the initial free-surface level is prescribed by patching the cell zones: cells below the specified level are assigned to the water phase, while cells above it are assigned to the air phase. In other words, the water depth and the air region above the free surface are defined from the very beginning of the simulation through the Patch Cell-Zone procedure as illustrated in Fig. 7. The result of the hybrid initialization, including the distribution of the water and air phases, is now shown in the revised manuscript to make this setup clearer. In that figure, the patched regions illustrate the two-fluid configuration used in this study, and we have clarified in the numerical model section how the air phase is treated within the VOF formulation.

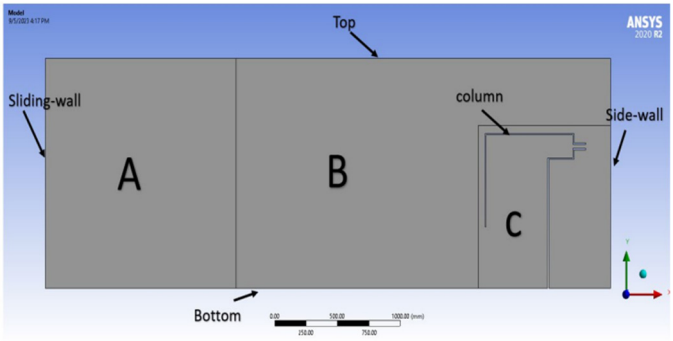

Fig. 6 Boundary conditions used in the CFD

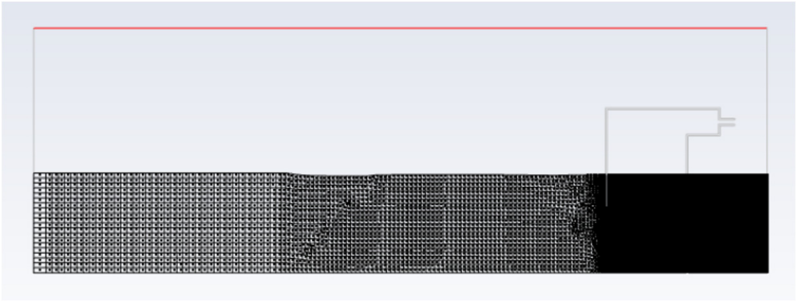

Fig. 7 Hybrid initialization region (water and air)

Table 1 Description of boundary condition

Boundary	Type	Method	Description
Sliding-wall	wall	no-slip	Used for dynamic mesh
Top	pressure outlet	Pressure outlet	Because the upper part consists of a free stream
Side-wall	wall	no-slip	Used for boundaries and dynamic mesh walls
Bottom	wall	no-slip	Because the flow is observed and the boundary layer is active
column	wall	no-slip	Because the flow is observed and the boundary layer is active

The wave-generating motion at the sliding wall was prescribed using a simplified sinusoidal wave displacement equation implemented via a User-Defined Function (UDF) in ANSYS Fluent. The wall motion equation is expressed in Eq. (7), and the corresponding angular velocity is given by Eq. (8). These expressions define the translational and rotational kinematics required to impose the desired regular wave pattern within a domain.

$$v = A.\omega.\cos\omega t \tag{7}$$

$$\omega = 2\pi f \tag{8}$$

Table 2 Characteristics of the wave

No	H (m)	T (s)	H/L	Pw (watt)
1	0.07	1.80	0.020	4.27
2	0.11	1.26	0.045	6.80
3	0.12	1.06	0.073	8.50
4	0.13	0.88	0.096	6.06

Table 3 Variable of the geometry

Model Geometry	Rectangular	Orifice Ratio 0.0130
		Orifice Ratio 0.0079
		Orifice Ratio 0.0040
	Rounded-Case	Orifice Ratio 0.0130
		Orifice Ratio 0.0079
		Orifice Ratio 0.0040
	Quarter-Circle Case	Orifice Ratio 0.0130
		Orifice Ratio 0.0079
		Orifice Ratio 0.0040
	Front-Semi Circle Case	Orifice Ratio 0.0130
		Orifice Ratio 0.0079
		Orifice Ratio 0.0040
	Back Semi Circle Case	Orifice Ratio 0.0130
		Orifice Ratio 0.079
		Orifice Ratio 0.0040
	Circle Case	Orifice Ratio 0.0130
		Orifice Ratio 0.0079
		Orifice Ratio 0.0040

where
v = velocity (m/s)
A = amplitude (m)
ω = angular frequency (rad/s)
t = time (s)
f = frequency (Hz)

The primary independent variable was the geometry of the OWC underlip. Eighteen variations were investigated, as listed in Table 3. These configurations are derived by combining different geometric shapes with three distinct orifice diameters. In addition, the baseline reference geometry is included for comparison. Each geometry was tested under multiple wave conditions, as specified in Table 2, to assess the performance sensitivity to both structural and hydrodynamic parameters.

2.4 Collecting and processing data

The simulations were conducted in a transient mode with a time-step size of 0.05 s, enabling detailed temporal resolution of the hydrodynamic variables. This time resolution allowed the collection of output data at 0.05-second intervals, ensuring accurate tracking of the oscillatory flow within the system. The output velocity and pressure were recorded by placing a virtual monitoring point that acted as a sensorat the outlet boundary of the OWC chamber. These readings form the basis for subsequent performance calculations.

Once the velocity and pressure time-series data were obtained, post-processing was performed to derive system performance parameters. The instantaneous pneumatic power was computed following the formulation presented by McCormick (2013) for Ocean Engineering, as expressed in Eq. (9). The system efficiency was evaluated using Eq. (10) with the available incident wave power determined from Eq. (11). Additionally, the orifice ratio for variable power takeoff (PTO) damping was determined using the relation given in Eq. (12).

$$P_u = (P_2 - P_0).v_2.A_2 \tag{9}$$

$$\eta = \frac{P_u}{P_w} \tag{10}$$

$$P_W = 0{,}195\, w\, \rho\, g\, h^2\, T \tag{11}$$

$$\tau = \frac{Ao}{Aw} \tag{12}$$

where:
P_u = pneumatic power extracted by the air flow (W)
P_w = incident wave power associated with the incoming waves over the device width (W)
η = hydrodynamic / wave-to-pneumatic efficiency
P_0 = atmospheric air pressure (Pa)
P_2 = air pressure at the upstream of the opening (Pa)
v_2 = mean air velocity through the duct or turbine section (m/s)
A_2 = cross-sectional flow area of the duct or turbine passage (m^2)
w = width of the device (m)
ρ = water density (kg/m^3)
h = wave height (m)
T = wave period (s)
τ = power take-off damping
A_o = cross-section of the orifice (m^2)
A_w = cross-section of the water column surface (m^2)

The output power of the system was derived from the measured velocity and pressure data, and the reference point for comparison was the maximum instantaneous power generated during the peak oscillation phase. This reference was chosen because, as discussed in the preceding section, velocity exhibited a stronger influence on output power than pressure when comparing the performance across configurations. Consequently, the efficiency calculations were based on the velocity measured at the peak oscillation, paired with the corresponding pressure values recorded at the same time step.

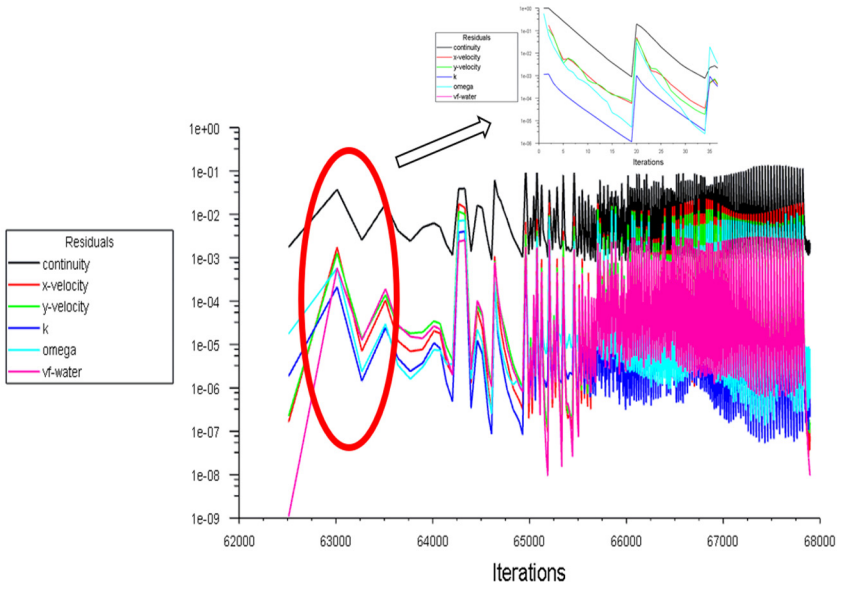

Fig. 8 Residual Iterations

3. Verification of simulation

All the simulations were executed using a residual convergence criterion of 0.001. A simulation was considered to converge when all monitored residuals fell below this threshold. As shown in Fig. 8, each time-step iteration required an average of 17 solver iterations, remaining within the predefined maximum of 20 iterations per time-step. This configuration ensured numerical stability and was deemed to be sufficient for accurate data acquisition.

Following the computation of the output power and system efficiency, the numerical results were validated against experimental data reported by Çelik (2022). The validation criterion was defined as a deviation of less than 10% between the simulated and experimental results. Fig. 9 presents the validation and verification outcomes, which indicate that the numerical model consistently achieved deviations below this threshold. Based on this level of agreement, the simulation results were considered valid and reliable for the subsequent detailed performance analyses.

4. Results and discussion

The processed data were analyzed to derive conclusions. This study focuses on the efficiency of the system and the underlying factors contributing to its improvement. In Figs. 9-12, the vertical axis represents the pneumatic efficiency. This is the ratio of the pneumatic power at the orifice (or turbine spot) to the incoming wave power. It measures how effectively wave energy is converted into airflow power at the exit of the chamber. This pneumatic efficiency is not the same as the total electrical efficiency of a wave energy converter. It does not account for losses in the turbine, generator, or power system.

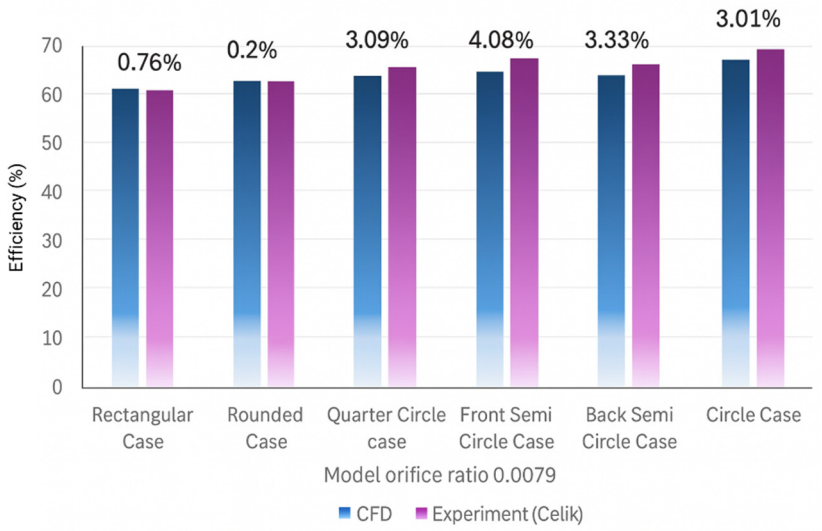

Fig. 9 Validation and verification of the simulation

4.1 Effect of geometry underlip

The maximum efficiencies corresponding to orifice ratios of 0.004, 0.0079, and 0.013 are presented in Figs. 10, 11, and 12, respectively. Across all orifice ratio variations, underlip modifications consistently improved the efficiency, exhibiting similar performance trends. The highest efficiency gain/improvement recorded at an orifice ratio of 0.013 reached 9.1%. This improvement was determined based on the ratio of the output power to the incident-wave power at the system outlet. Among all the tested configurations, the circular underlip model achieved the highest efficiency, attributed to its ability to generate the largest output power.

This finding is particularly noteworthy because it demonstrates that a relatively minor geometric modification, limited to the underlip, can yield efficiency gain/improvement of up to 9.1%. Further analysis was performed to elucidate the underlying mechanism responsible for this enhancement. Turbulent kinetic energy (TKE) has been identified as a key factor influencing OWC performance. In conventional designs, an excessive TKE contributes to energy dissipation through friction and chaotic flow patterns, thereby reducing the amount of wave energy available for conversion at the output. The circular underlip configuration appears to mitigate these losses, enabling more effective energy capture and, consequently, a higher overall efficiency.

4.2 Hydrodynamic phenomena on device

To visually identify and investigate the causes of the observed increase in system efficiency, computational flow visualizations were generated in the form of turbulent kinetic energy (TKE) contours and pathlines. The TKE pathlines were used to analyze the flow patterns, evaluate the turbulence intensity, and determine the mechanisms contributing to efficiency enhancement. In this study, TKE analysis forms the core of the discussion, as it directly indicates the magnitude and location of the flow energy losses within the Oscillating Water Column (OWC) system.

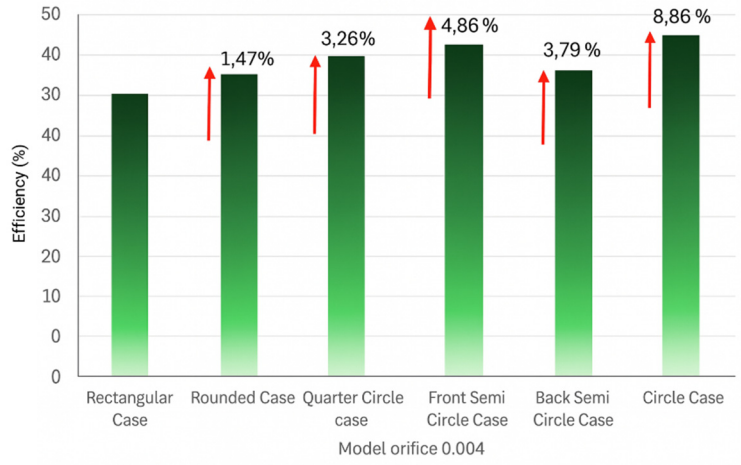

Fig. 10 Efficiency model on orifice 0.004

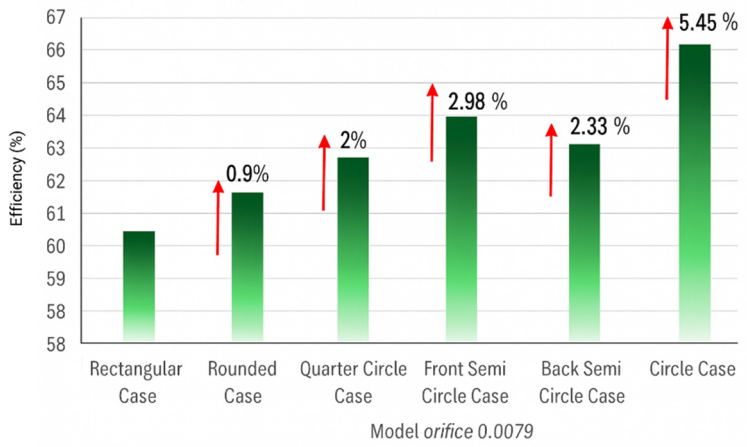

Fig. 11 Efficiency model on orifice 0.0079

The investigation was conducted for each wave condition and orifice ratio; however, a detailed discussion is limited to the 0.004 orifice ratio, as the flow patterns for other ratios were qualitatively similar, differing primarily in the magnitude of the TKE. Fig. 13 illustrates the TKE path for the rectangular underlip model. This configuration exhibited the largest turbulence concentration in the underlip region, as indicated by the high-intensity color zones. The sharp geometry promoted random flow separation when waves passed along the underlip edge, leading to significant TKE generation. This turbulence increases the wall friction within the column and dissipates the wave energy before it reaches the outlet. Consequently, the overall efficiency of the system is reduced. Furthermore, the presence of strong recirculation zones disrupts the resonance between incoming ocean waves and the vertical oscillation of water within the column.

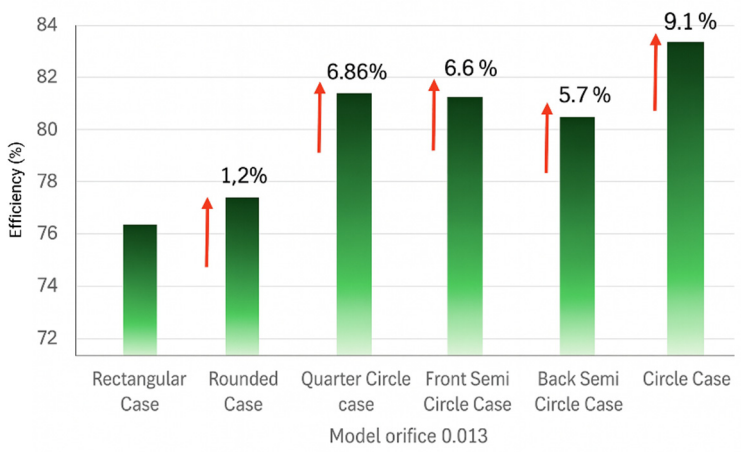

Fig. 12 Efficiency model on orifice 0.013

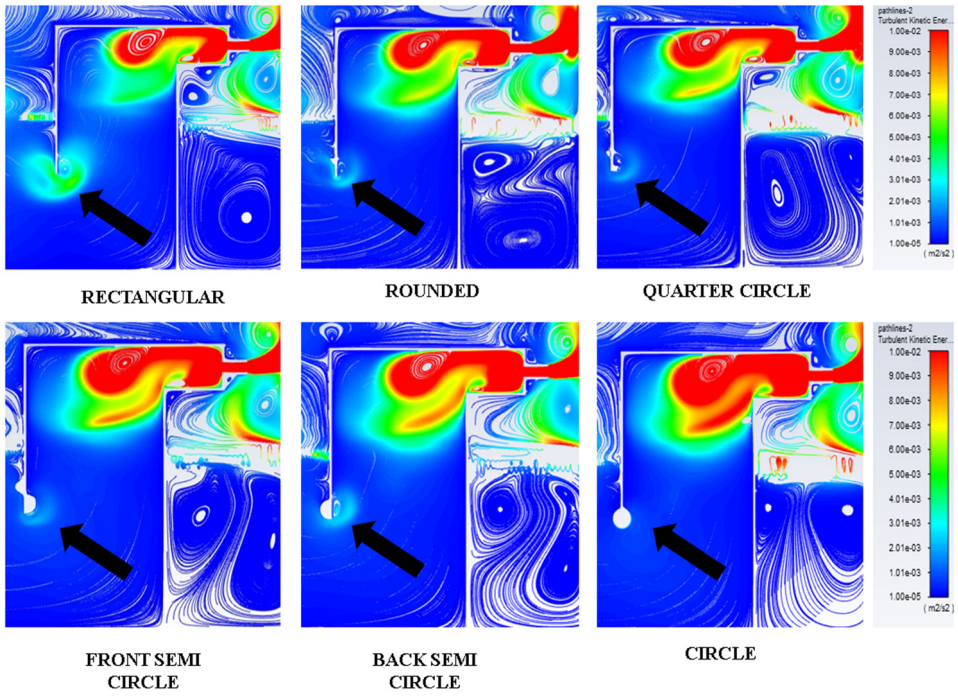

Fig. 13 Turbulent kinetic energy (wave coming to the device)

In contrast, the rounded underlip modification (Fig. 13) shows a reduction in the TKE magnitude compared with the rectangular design, although the turbulence remains higher than in other curved configurations. Here, turbulence is localized mainly within the underlip region, allowing for slightly improved energy transfer. However, a significant clamping flow still occurs during the wave exit, potentially interrupting the flow resonance for subsequent waves. The

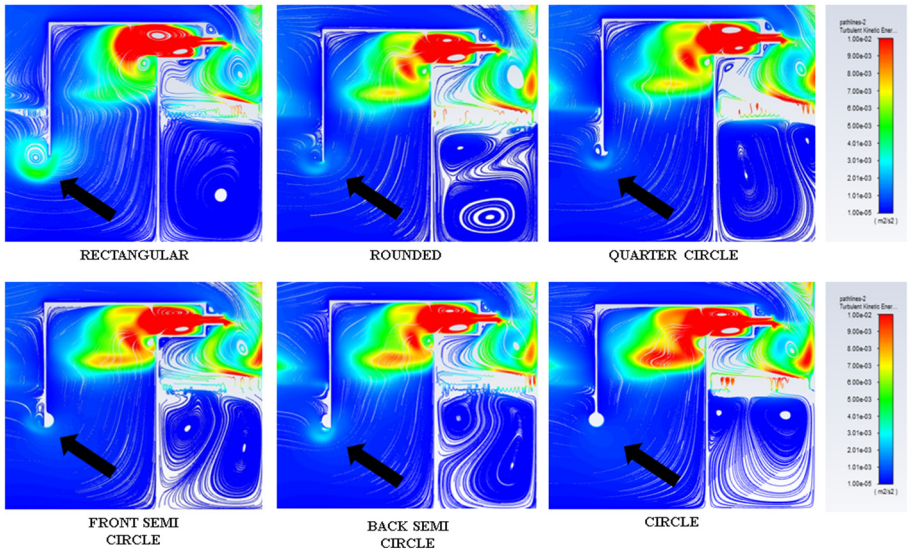

Fig. 14 Turbulence kinetic energy (wave back from the device)

quarter-circle model exhibits a further reduction in turbulence, with the TKE concentration shifting toward the rear geometry during wave entry. This reduction in turbulence corresponds to a modest increase in efficiency compared to both the rectangular and rounded configurations.

The front semi-circular underlip modification displayed even lower TKE levels in the underlip region, as confirmed by the color spectrum. The smooth curvature reduces the flow separation during wave entry. However, during wave return, the localized flow rotation at the column front generates new turbulence, which can weaken the resonance conditions. Conversely, the rear semi-circular underlip shows good inflow patterns but suffers from elevated TKE inside the column during wave entry, lowering the efficiency compared with the front semi-circular model.

The circular underlip configuration demonstrated the most favorable results. Its continuous curvature minimizes random flow rotation, substantially reducing the turbulence generation. This design effectively prevents excessive TKE buildup, allowing wave energy to be transmitted more efficiently to the outlet. Consequently, this model achieved the highest efficiency among all configurations tested.

Similar trends were observed during wave return (Fig. 14): the rectangular underlip consistently produced the highest TKE levels, whereas the circular underlip maintained the lowest turbulence. The key mechanisms influencing the efficiency are linked to the presence of hydraulic jumps and flow separation within the OWC. Sharp-edged geometries, such as the rectangular underlip, promote sudden hydraulic jumps and unstable velocity and pressure distributions, leading to random, undirected flow, and elevated TKE. In contrast, the circular underlip minimizes these phenomena by maintaining a smooth, stable velocity field and reducing abrupt transitions between the supercritical and subcritical flow regimes.

Overall, the TKE contour and pathline analyses confirm that reducing turbulence, primarily by minimizing hydraulic jumps and flow separation, significantly improves the energy transfer efficiency. The circular underlip modification proved to be the most effective design, achieving the most stable flow field and highest conversion efficiency.

Under representative wave conditions and a specific underlip configuration, the free-surface elevation within the chamber demonstrated a bounded oscillation, characterized by distinct minimum and maximum levels during each wave cycle. The corresponding excursion was entirely contained within the chamber, remaining below the roof and above the lip depth, thereby preventing both overtopping and drying out under the simulated conditions. This behavior suggests that the motion of the internal water column is predominantly influenced by resonance and PTO damping, establishing a direct physical connection between the observed pneumatic efficiency trends and underlying hydrodynamics.

5. Conclusions

This study investigated the influence of the underlip geometry on the performance of an Oscillating Water Column (OWC) system. The key findings are summarized as follows.

- The geometry of the front wall of the column (underlip), as modified in this study, significantly affected the efficiency of the OWC system. Among all configurations tested, the circular underlip model consistently achieved the highest efficiency gains. Overall, all the tested modifications, including the rectangular underlip, rounded underlip, quarter-circle underlip, front semi-circular underlip, back semi-circular underlip, and circular underlip, contributed to performance improvements, although the magnitude of improvement varied. The highest improvement efficiency in this research was 9.1% for an orifice ratio of 0.013.
- The underlip geometry strongly influences the internal flow patterns of the OWC system. Unfavorable flow patterns are associated with elevated turbulent kinetic energy, which leads to performance loss. The introduction of appropriately designed underlip modifications reduces the turbulent kinetic energy, thereby improving energy transfer and overall system efficiency.

Acknowledgments

The authors wish to extend their sincere gratitude to all the parties who contributed to the successful completion of this research, with special appreciation to Azhar Bima Alfarozi for his valuable assistance as a research assistant. This study was funded by the Faculty of Engineering, Universitas Gadjah Mada (grant no. 1800612/UN1.FTK/SK/HK/2024).

References

Carlo, L., Iuppa, C. and Faraci, C. (2023), “A numerical-experimental study on the hydrodynamic performance of a U-OWC wave energy converter”, *Renew. Energ.*, **203**, 89-101. https://doi.org/10.1016/j.renene.2022.12.057.

Çelik, A. (2022), “An experimental investigation into the effects of front wall geometry on OWC performance for various levels of applied power take off dampings”, *Ocean Eng.*, **248**, 110761. https://doi.org/10.1016/j.oceaneng.2022.110761.

Çelik, A. and Altunkaynak, A. (2021), “An in depth experimental investigation into effects of incident wave characteristics front wall opening and PTO damping on the water column displacement and air differential pressure in an OWC chamber”, *Energy*, **230**, 120827. https://doi.org/10.1016/j.energy.2021.120827.

Fleming, A.N. and Macfarlane, G.J. (2017), "Experimental flow field comparison for a series of scale model oscillating water column wave energy converters", *Mar. Struct.*, **52**, 108-125. https://doi.org/10.1016/j.marstruc.2016.12.005.

Güths, A.K., Teixeira, P.R.F. and Didier, E. (2022), "A novel geometry of an onshore Oscillating Water Column wave energy converter", *Renew. Energ.*, **201**, 938-949. https://doi.org/10.1016/j.renene.2022.10.121

John Ashlin, S., Sundar, V. and Sannasiraj, S.A. (2016), "Effects of bottom profile of an oscillating water column device on its hydrodynamic characteristics", *Renew. Energ.*, **96**, 341-353. https://doi.org/10.1016/j.renene.2016.04.091.

Kamath, A., Bihs, H. and Arntsen, ˜I.A. (2014), "Comparison of 2D and 3D Simulations of OWC In different configurations", *Coast. Eng. Proceedings*, **34**, 66. https://doi.org/10.9753/icce.v34.structures.66.

Koo, W.C. and Kim, M.H. (2012), "A time-domain simulation of an oscillating water column with irregular waves", *Ocean Syst. Eng.*, **2**(2), 147-158. https://doi.org/10.12989/ose.2012.2.2.147.

Mandev, M.B. and Altunkaynak, A. (2023), "Cylindrical frontwall entrance geometry optimization of an oscillating water column for utmost hydrodynamic performance", *Energy*, **280**, 128147. https://doi.org/10.1016/j.energy.2023.128147.

McCormick, M.E. (2013). *Ocean Wave Energy Conversion*. Dover Publications.

Mia, M.R., Zhao, M., Wu, H. and Munir, A. (2022), "Numerical investigation of offshore oscillating water column devices", *Renew. Energ.*, **191**, 380-393. https://doi.org/10.1016/j.renene.2022.04.069.

Mohapatra, P., Vijay, K.G., Bhattacharyya, A. and Sahoo, T. (2023), "Influence of distinct bottom geometries on the hydrodynamic performance of an OWC device", *Energy*, **277**, 127605. https://doi.org/10.1016/j.energy.2023.127605.

Monteiro, W.M.L., de Almeida Sarmento, A.J.N., Monteiro, J.A.L., Semedo, B.R., Carvalho, A.B. and Furtado, T.T. (2025), "The influence of flow damping on the maritime natural cave performance", *Ocean Syst. Eng.*, **15**(2), 153-171. https://doi.org/10.12989/ose.2025.15.2.153.

Ning, D., Mu, D., Wang, R. and Mayon, R. (2023), "Experimental and numerical investigations on the solitary wave actions on a land-fixed OWC wave energy converter", *Energy*, **282**, 128363. https://doi.org/10.1016/j.energy.2023.128363.

Prasanna, S., Bae, Y.H. and Kumar, P.S. (2025), "Data-driven design and optimization of multi-chamber oscillating water column using CFD and machine learning", *Ocean Syst. Eng.*, **15**(2), 173-194. https://doi.org/10.12989/ose.2025.15.2.173.

Qu, M., Yu, D., Xu, Z. and Gao, Z. (2022), "The effect of the elliptical front wall on energy conversion performance of the offshore OWC chamber: A numerical study", *Energy*, **255**, 124428. https://doi.org/10.1016/j.energy.2022.124428.

Vyzikas, T., Deshoulières, S., Giroux, O., Barton, M. and Greaves, D. (2017), "Numerical study of fixed Oscillating Water Column with RANS-type two-phase CFD model", *Renew. Energ.*, **102**, 294-305. https://doi.org/10.1016/j.renene.2016.10.044.

Wang, C., Zhang, Y. and Deng, Z. (2022), "Wave power extraction for an oscillating water column device consisting of a surging front and back lip-wall: An analytical study", *Renew. Energ.*, **184**, 100-114. https://doi.org/10.1016/j.renene.2021.11.070.

Zeng, Y., Shi, W., Michailides, C., Ren, Z. and Li, X. (2022), "Turbulence model effects on the hydrodynamic response of an oscillating water column (OWC) with use of a computational fluid dynamics model", *Energy*, **261**, 124926. https://doi.org/10.1016/j.energy.2022.124926.

Zhou, Y., Ning, D., Chen, L. and Iglesias, G. (2021), "Nonlinear hydrodynamic modeling of an offshore stationary multi-oscillating water column platform", *Ocean Eng.*, **227**, 108919. https://doi.org/10.1016/j.oceaneng.2021.108919.